Activity of Protein Kinase RIPK3 Determines Whether Cells Die by Necroptosis or Apoptosis

Kim Newton,[1]* Debra L. Dugger,[1] Katherine E. Wickliffe,[1] Neeraj Kapoor,[1] M. Cristina de Almagro,[2] Domagoj Vucic,[2] Laszlo Komuves,[3] Ronald E. Ferrando,[3] Dorothy M. French,[3]† Joshua Webster,[3] Merone Roose-Girma,[4] Søren Warming,[4] Vishva M. Dixit[1]*

Receptor-interacting protein kinase 1 (RIPK1) and RIPK3 trigger pro-inflammatory cell death termed "necroptosis." Studies with RIPK3-deficient mice or the RIPK1 inhibitor necrostatin-1 suggest that necroptosis exacerbates pathology in many disease models. We engineered mice expressing catalytically inactive RIPK3 D161N or RIPK1 D138N to determine the need for the active kinase in the whole animal. Unexpectedly, RIPK3 D161N promoted lethal RIPK1- and caspase-8–dependent apoptosis. In contrast, mice expressing RIPK1 D138N were viable and, like RIPK3-deficient mice, resistant to tumor necrosis factor (TNF)–induced hypothermia. Cells expressing RIPK1 D138N were resistant to TNF-induced necroptosis, whereas TNF-induced signaling pathways promoting gene transcription were unperturbed. Our data indicate that the kinase activity of RIPK3 is essential for necroptosis but also governs whether a cell activates caspase-8 and dies by apoptosis.

Tumor necrosis factor receptor 1 (TNFR1), Toll-like receptors (TLRs), and antigen receptors trigger necroptotic cell death when caspase-8 is inhibited and cells express receptor-interacting protein kinase 3 (RIPK3) and its substrate MLKL (mixed lineage kinase domain-like) (*1*). Wild-type RIPK3, but not catalytically inactive RIPK3 mutants, can reconstitute necroptosis in RIPK3-deficient cells (*2*–*4*), indicating that the kinase activity of RIPK3 is critical. TNFR1 engages RIPK3 through RIPK1, whereas TRIF (Toll/interleukin-1 receptor domain–containing adaptor inducing interferon-β) links RIPK3 to TLRs 3 and 4 (*1*). In the absence of antibodies that label cells dying by necroptosis, the contribution of necroptosis to pathology has been inferred from the resistance of $Ripk3^{-/-}$ mice to pancreatitis, retinal degeneration, atherosclerosis, liver injury, and systemic inflammation (*1*). The caveat here is that loss of RIPK3 could indicate a scaffold function for RIPK3 rather than a requirement for its kinase activity. Necrostatin-1 (nec-1) inhibits RIPK1 and ameliorates disease in some animal models too, although nec-1 might also inhibit other cellular processes via inhibition of indoleamine 2,3 dioxygenase (*5*).

We sought genetic proof that the kinase activity of RIPK3 drives necroptosis and disease by generating *Ripk3* knock-in mice with Asp^{161} of the catalytically important DFG motif mutated to Asn (fig. S1, A and B). Whereas $Ripk3^{-/-}$ mice are viable (*6*), $Ripk3^{D161N/D161N}$ mice died around embryonic day 11.5 (E11.5) with abnormal yolk sac vasculature (Fig. 1, A and B). (Single-letter abbreviations for the amino acid residues are as follows: D, Asp; N, Asn. In the mutants, other amino acids were substituted at certain locations; for example, D161N indicates that aspartic acid at position 161 was replaced by asparigine.) Staining for the endothelial cell marker PECAM-1 (platelet/endothelial cell adhesion molecule 1) and cleaved caspase-3, a marker of apoptosis, revealed significantly increased apoptosis in the $Ripk3^{D161N/D161N}$ yolk sac vasculature (Fig. 1C). RIPK3 is expressed in endothelial cells and gut epithelial cells during development (fig. S1C). $Ripk3^{D161N/-}$ mice, which are expected

[1]Department of Physiological Chemistry, Genentech, 1 DNA Way, South San Francisco, CA 94080, USA. [2]Department of Early Discovery Biochemistry, Genentech, 1 DNA Way, South San Francisco, CA 94080, USA. [3]Department of Pathology, Genentech, 1 DNA Way, South San Francisco, CA 94080, USA. [4]Department of Molecular Biology, Genentech, 1 DNA Way, South San Francisco, CA 94080, USA.

*Corresponding author. E-mail: knewton@gene.com (K.N.); dixit@gene.com (V.M.D.)

†Present address: Gilead Sciences, 333 Lakeside Drive, Foster City, CA 94404, USA.

Fig. 1. $Ripk3^{D161N/D161N}$ mice die during embryogenesis. (**A**) Numbers of surviving offspring from $Ripk3^{D161N/+}$ parents. Mouse strains were derived from independent $Ripk3^{D161N/+}$ embryonic stem cell clones. (**B**) E11.5 embryos and their yolk sacs. (**C**) E11.5 yolk sacs stained for PECAM-1 (red) and cleaved caspase-3 (CC3) (green). Scale bar, 200 μm. Each square in the scatter plot represents the yolk sac of one embryo. $CC3^+$ cells were counted in 8 to 17 fields per embryo, and the mean number per field is plotted. *P* value determined with Student's *t* test.

A

Strain	$Ripk3^{+/+}$	$Ripk3^{D161N/+}$	$Ripk3^{D161N/D161N}$
1	86	151	0
2	45	88	0
3	9	14	0

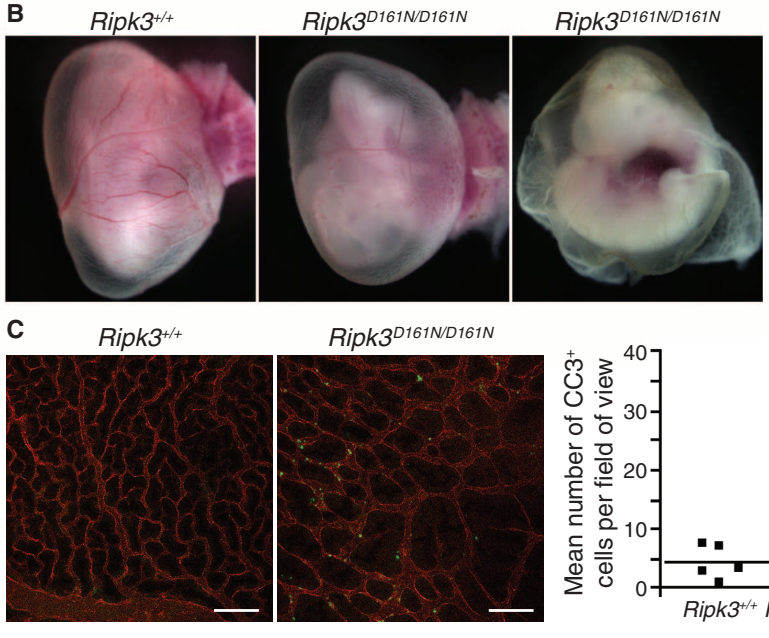

Fig. 2. RIPK1- and caspase-8–dependent embryonic lethality caused by RIPK3 D161N. (**A**) Proposed mechanism for control of necroptosis and apoptosis by RIPK3 and RIPK3 D161N. (**B**) Numbers of surviving offspring from *Casp8*$^{+/-}$ *Ripk3*$^{D161N/+}$ parents. (**C**) Spleen and lymph nodes from mice aged 16 to 20 weeks. Scale bar, 1 cm. (**D**) Leukocytes in the spleen or brachial, inguinal, mesenteric, and axillary lymph nodes were counted. Bars represent the mean ± SD. (**E**) Numbers of P3 to P6 offspring from *Ripk1*$^{+/-}$ *Ripk3*$^{D161N/+}$ parents. (**F**) E18.5 littermates.

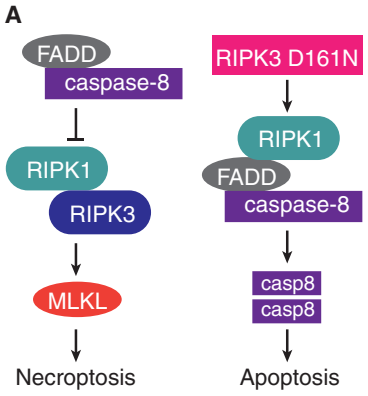

B	*Ripk3*$^{+/+}$	*Ripk3*$^{D161N/+}$	*Ripk3*$^{D161N/D161N}$
Casp8$^{+/+}$	32	56	0
Casp8$^{+/-}$	51	140	0
Casp8$^{-/-}$	0	0	30

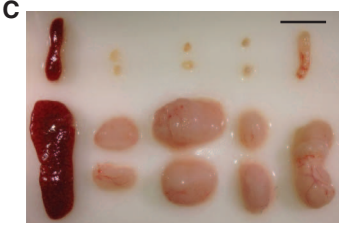

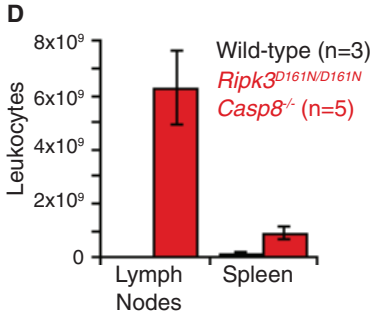

E	*Ripk3*$^{+/+}$	*Ripk3*$^{D161N/+}$	*Ripk3*$^{D161N/D161N}$
Ripk1$^{+/+}$	16	20	0
Ripk1$^{+/-}$	24	45	0
Ripk1$^{-/-}$	0	0	2

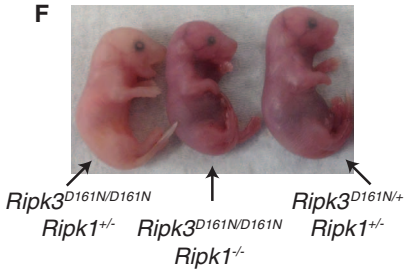

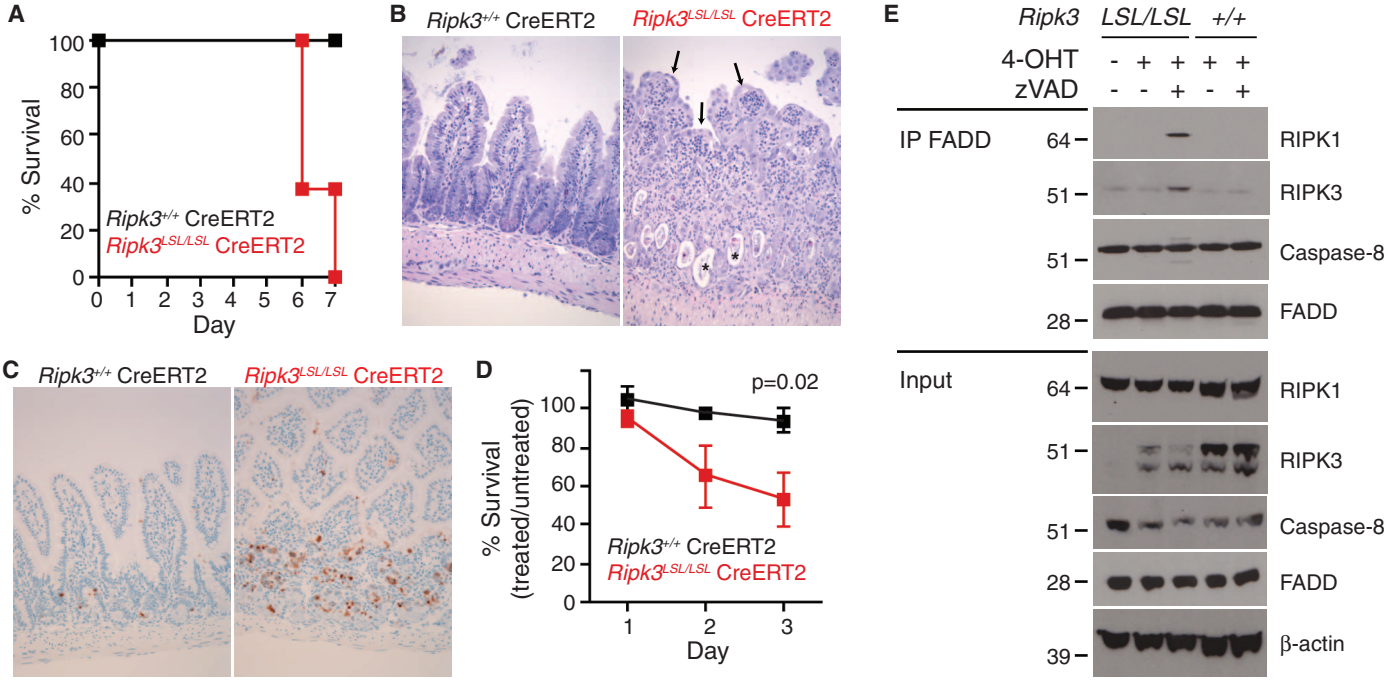

Fig. 3. Lethal effect of RIPK3 D161N expressed in adult mice. (**A**) Effect of tamoxifen-induced RIPK3 D161N expression on adult mouse survival. Mice (n = 8 per genotype) received daily tamoxifen injections on days 1 through 5. (**B**) Hematoxylin and eosin stained small intestine on day 7. Arrows indicate blunted and fused villi. Asterisks indicate crypt degeneration. Magnification is 20×. (**C**) Small intestine harvested on day 5. Cells expressing cleaved caspase-3 are stained brown. Magnification is 20×. (**D**) Survival of MEFs cultured in 4-hydroxytamoxifen (4-OHT). Percent survival = 100 × [percent viable cells (unstained by propidium iodide) after 4-OHT treatment]/[percent viable cells in medium alone]. Data represent the mean ± SD of three lines per genotype. P value on day 3 determined with Student's t test. (**E**) Western blots of FADD-containing protein complexes immunoprecipitated from CreERT2 MEFs cultured for 2 days in medium, 4-OHT, or 4-OHT and zVAD.fmk.

to make half the amount of RIPK3 D161N, were viable. Therefore, there may be a threshold above which the RIPK3 D161N protein becomes lethal. *Ripk3*$^{D161N/+}$ mice had a normal life span, arguing against RIPK3 D161N acting as a dominant negative mutant.

The genetic evidence for caspase-8 and its adaptor FADD (Fas-associated via death domain) inhibiting necroptosis caused by RIPK1 and RIPK3 is compelling (*1*). We tested whether RIPK3 D161N promoted caspase-8–dependent apoptosis (Fig. 2A) by breeding the *Ripk3*^{D161N} allele onto a caspase-8–null background (fig. S2A). *Casp8*$^{-/-}$ embryos, like *Ripk3*$^{D161N/D161N}$ embryos, die mid-gestation (*7*), but double mutant *Casp8*$^{-/-}$ *Ripk3*$^{D161N/D161N}$ mice were viable (Fig. 2B). Halving the *Casp8* gene dosage delayed lethality until ~E15.5 (fig. S2B). *Casp8*$^{-/-}$ *Ripk3*$^{D161N/D161N}$ mice resembled *Casp8*$^{-/-}$ *Ripk3*$^{-/-}$ mice (*8*, *9*) because they accumulated T cells expressing the surface markers CD3 and B220 (fig. S2C) and developed the lymphadenopathy and splenomegaly (Fig. 2, C and D) that is characteristic of impaired apoptosis signaling by the death receptor Fas. These data confirm that (i) RIPK3 D161N promotes caspase-8–dependent apoptosis during embryogenesis and (ii) the kinase activity of RIPK3 is required for the death of *Casp8*$^{-/-}$ embryos. The kinase activity of RIPK3 also appears to mediate the proliferation defect of *Casp8*$^{-/-}$ T cells (*10*) because *Casp8*$^{-/-}$ *Ripk3*$^{D161N/D161N}$ T cells proliferated normally in response to antibodies to CD3 and CD28 (fig. S2D).

Although a direct interaction between RIPK3 D161N and caspase-8 during embryogenesis is a possibility, we think that RIPK3 may influence caspase-8 through RIPK1 and FADD. RIPK3 and RIPK1 interact via their RIP homotypic interaction motifs (RHIMs) (*11*); RIPK1 and FADD can interact through their death domains (*12*); and FADD and caspase-8 interact through their death effector domains (*13*). Consistent with this model, RIPK1 deficiency (fig. S3A) rescued embryonic lethality caused by RIPK3 D161N (Fig. 2, E and F). *Ripk1*$^{-/-}$ mice died soon after birth with increased cell death in the colon, brown adipose tissue, and thymus (fig. S3B). RIPK1 is abundant in the wild-type intestine at E18.5 and can also be detected in brown fat and liver (fig. S3C). *Ripk1*$^{-/-}$ *Ripk3*$^{D161N/D161N}$ mice died soon after birth with the same intestinal lesions as *Ripk1*$^{-/-}$ mice (fig. S3B), suggesting that the defects caused by RIPK1 loss do not require RIPK3-dependent necroptosis. Halving the *Ripk1* gene dosage delayed death due to RIPK3 D161N (Fig. 2F). At E18.5, pale *Ripk1*$^{+/-}$ *Ripk3*$^{D161N/D161N}$ embryos exhibited none of the lesions associated with RIPK1 loss but contained fewer hematopoietic cells and less hepatic glycogen (fig. S3D). *Ripk3*$^{D161N/D161N}$ embryos lacking MLKL, TRIF, the RHIM protein DAI (DNA-dependent activator of interferon-regulatory factors), the RIPK1 deubiquitinase CYLD (cylindromatosis), TNFR1, DR3 (death receptor 3), or FLIP (FLICE-inhibitory protein) did not survive beyond ~E11.5 (fig. S4), indicating that these proteins are dispensable for activation of caspase-8 by RIPK3 D161N.

To test whether RIPK3 D161N was deleterious in adult mice, we engineered *Ripk3*$^{LSL/LSL}$ mice with *loxp*-Stop-*loxp* (LSL) transcription termination cassettes preventing expression of RIPK3 D161N during development (fig. S1B). This strategy was possible because *Ripk3*$^{-/-}$ mice develop normally (*6*). We deleted the LSL cassettes and switched on expression of RIPK3 D161N in adults using ubiquitously expressed tamoxifen-inducible cre recombinase (CreERT2) (*14*). All *Ripk3*$^{LSL/LSL}$ CreERT2 mice given tamoxifen developed diarrhea and lost between 13 and 28% of their body weight after 6 to 7 days, requiring that they be euthanized. No morbidity was observed in *Ripk3*$^{+/+}$ or *Ripk3*$^{LSL/+}$ mice expressing CreERT2 (Fig. 3A and fig. S5A). Histological analyses of *Ripk3*$^{LSL/LSL}$ CreERT2 mice revealed degeneration of intestinal crypts, villous blunting and fusion, and mild enteritis (Fig. 3B). Lesions were mainly in the small intestine. Many mice had segmental, submucosal edema in the large intestine. Pyknotic and karyorrhectic lymphocytes in secondary lymphoid organs and thymic atrophy were consistent with lymphocyte death (fig. S5B). *Ripk3*$^{LSL/LSL}$ CreERT2 mice showed no signs of morbidity after 5 days, but staining for cleaved caspase-3 revealed increased apoptosis in the small intestine (Fig. 3C). These results suggest that RIPK3 D161N affects caspase-8 in the small intestine like it does in the embryo vasculature.

We sought biochemical evidence of RIPK3 D161N affecting caspase-8 in *Ripk3*$^{LSL/LSL}$ CreERT2 mouse embryo fibroblasts (MEFs) immortalized with adenovirus E1A. Culture with 4-hydroxytamoxifen, to promote expression of RIPK3 D161N, caused increased cell death that was not seen in *Ripk3*$^{+/+}$ CreERT2 cultures (Fig. 3D). This death appeared to be apoptosis because it was blocked by the pan-caspase inhibitor zVAD.fmk (carbobenzoxy-valyl-alanyl-aspartyl-[O-methyl]-fluoromethylketone), but not by nec-1 (fig. S5C). As a control, nec-1 blocked the death of wild-type E1A-immortalized MEFs treated with TNF/zVAD.fmk (fig. S5D). Inhibition of apoptosis caused by RIPK3 D161N allowed us to isolate a complex containing FADD, caspase-8, RIPK1, and RIPK3 D161N (Fig. 3E). An equivalent complex was not recovered from similarly treated *Ripk3*$^{+/+}$ CreERT2^{+} cells. Further emphasizing the ability of RIPK3 D161N to promote apoptosis, the mutant RIPK3 protein was less abundant than was wild-type RIPK3. Poor expression of RIPK3 D161N did not result from decreased transcription of *Ripk3*^{D161N} mRNA (fig. S5E). In the absence of structural data for RIPK3 D161N, it is unclear why this catalytically inactive mutant engages RIPK1, FADD, and caspase-8 but wild-type RIPK3 does not. Regardless, our results indicate that the kinase activity of RIPK3 dictates whether a cell dies from necroptosis

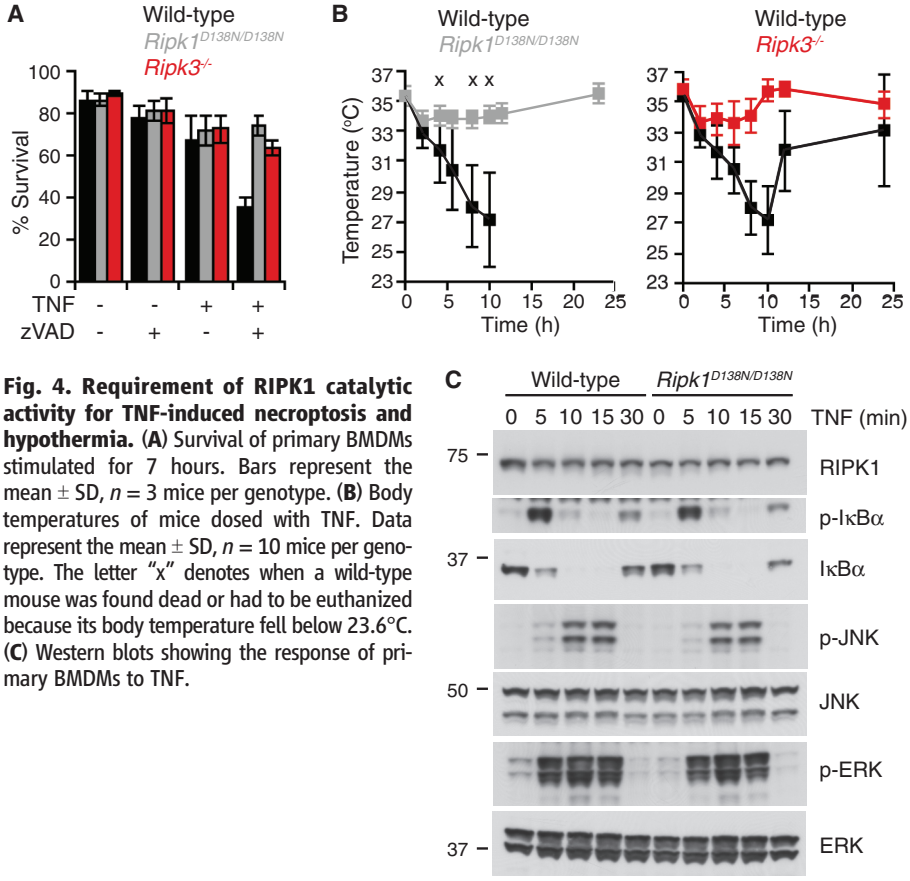

Fig. 4. Requirement of RIPK1 catalytic activity for TNF-induced necroptosis and hypothermia. (**A**) Survival of primary BMDMs stimulated for 7 hours. Bars represent the mean ± SD, $n = 3$ mice per genotype. (**B**) Body temperatures of mice dosed with TNF. Data represent the mean ± SD, $n = 10$ mice per genotype. The letter "x" denotes when a wild-type mouse was found dead or had to be euthanized because its body temperature fell below 23.6°C. (**C**) Western blots showing the response of primary BMDMs to TNF.

or apoptosis. As such, small-molecule inhibitors of RIPK3 may have limited therapeutic benefit because of their potential to promote apoptotic cell death.

Nec-1 blocked necroptosis induced by TNF/zVAD.fmk (fig. S5C), was protective in an inflammatory disease model (*15*), and does not induce apoptotic cell death, suggesting that inhibition of RIPK1 rather than RIPK3 may have therapeutic benefit. To mimic RIPK1 inhibition in the whole animal, we generated *Ripk1* knock-in mice with Asp^{138} of the HKD motif necessary for kinase activity mutated to Asn (fig. S6, A and B). Whereas $Ripk1^{-/-}$ mice died soon after birth, $Ripk1^{D138N/D138N}$ mice were viable. Consistent with a critical role for the kinase activity of RIPK1 in TNF-induced necroptosis, $Ripk1^{D138N/D138N}$ bone marrow–derived macrophages (BMDMs) and E1A-immortalized MEFs were as resistant as $Ripk3^{-/-}$ cells to killing by TNF/zVAD.fmk (Fig. 4A and fig. S6C). $Ripk1^{D138N/D138N}$ cells expressed normal amounts of RIPK3 and MLKL (Fig. S6D). $Ripk1^{D138N/D138N}$ mice also resembled $Ripk3^{-/-}$ mice in their systemic response to TNF, exhibiting less hypothermia than did their wild-type counterparts (Fig. 4B). Unlike RIPK1 loss, RIPK1 D138N did not rescue embryonic lethality caused by RIPK3 D161N (fig. S4). This result is consistent with nec-1 not protecting MEFs expressing RIPK3 D161N (fig. S5B) and indicates that the kinase activity of RIPK1 is not required for activation of caspase-8 by RIPK3 D161N.

RIPK1 is required for TNF-induced nuclear factor κB (NF-κB) and mitogen-activated protein kinase signaling (*16*, *17*). Wild-type RIPK1 and RIPK1 D138N restored these signals in $Ripk1^{-/-}$ cells (*18*), suggesting that RIPK1 has an essential scaffold function in this setting, whereas its kinase activity is dispensable. Indeed, $Ripk1^{D138N/D138N}$ and wild-type BMDMs were indistinguishable in their phosphorylation of inhibitor of NF-κB α (IκBα), c-Jun N-terminal kinase (JNK), and extracellular signal-regulated kinase (ERK) in response to TNF (Fig. 4C). These results, together with the viability of $Ripk1^{D138N/D138N}$ mice, are encouraging because they suggest that inhibiting the kinase activity of RIPK1 has no deleterious effects, at least in the short term. These $Ripk1^{D138N/D138N}$ mice can be used to explore the contribution of RIPK1 and necroptosis to various mouse models of human disease.

References and Notes

1. K. Moriwaki, F. K. Chan, *Genes Dev.* **27**, 1640–1649 (2013).
2. Y. S. Cho *et al.*, *Cell* **137**, 1112–1123 (2009).
3. S. He *et al.*, *Cell* **137**, 1100–1111 (2009).
4. D. W. Zhang *et al.*, *Science* **325**, 332–336 (2009).
5. N. Takahashi *et al.*, *Cell Death Dis.* **3**, e437 (2012).
6. K. Newton, X. Sun, V. M. Dixit, *Mol. Cell. Biol.* **24**, 1464–1469 (2004).
7. E. E. Varfolomeev *et al.*, *Immunity* **9**, 267–276 (1998).
8. A. Oberst *et al.*, *Nature* **471**, 363–367 (2011).
9. W. J. Kaiser *et al.*, *Nature* **471**, 368–372 (2011).
10. L. Salmena *et al.*, *Genes Dev.* **17**, 883–895 (2003).
11. X. Sun, J. Yin, M. A. Starovasnik, W. J. Fairbrother, V. M. Dixit, *J. Biol. Chem.* **277**, 9505–9511 (2002).
12. Y. H. Park, M. S. Jeong, H. H. Park, S. B. Jang, *Biochim. Biophys. Acta* **1834**, 292–300 (2013).
13. M. Muzio *et al.*, *Cell* **85**, 817–827 (1996).
14. J. Seibler *et al.*, *Nucleic Acids Res.* **31**, e12 (2003).
15. L. Duprez *et al.*, *Immunity* **35**, 908–918 (2011).
16. M. A. Kelliher *et al.*, *Immunity* **8**, 297–303 (1998).
17. T. H. Lee *et al.*, *Mol. Cell. Biol.* **23**, 8377–8385 (2003).
18. T. H. Lee, J. Shank, N. Cusson, M. A. Kelliher, *J. Biol. Chem.* **279**, 33185–33191 (2004).

Acknowledgments: We thank J. Starks, K. O'Rourke, A. Maltzman, M. Schlatter, T. Soukup, L. Tam, R. Pattni, R. Newman, H. Ngu, and D. Siler for technical assistance. S. Sun, W. Alexander, S. Akira, and Y. He kindly provided knockout mice. All authors were employees of Genentech.

Supplementary Materials

www.sciencemag.org/content/343/6177/1357/suppl/DC1
Materials and Methods
Figs. S1 to S6
References (*19*–*25*)

5 December 2013; accepted 6 February 2014
Published online 20 February 2014;
10.1126/science.1249361

Highly Multiplexed Subcellular RNA Sequencing in Situ

Je Hyuk Lee,[1,2]*† Evan R. Daugharthy,[1,2,4]* Jonathan Scheiman,[1,2] Reza Kalhor,[2] Joyce L. Yang,[2] Thomas C. Ferrante,[1] Richard Terry,[1] Sauveur S. F. Jeanty,[1] Chao Li,[1] Ryoji Amamoto,[3] Derek T. Peters,[3] Brian M. Turczyk,[1] Adam H. Marblestone,[1,2] Samuel A. Inverso,[1] Amy Bernard,[5] Prashant Mali,[2] Xavier Rios,[2] John Aach,[2] George M. Church[1,2]†

Understanding the spatial organization of gene expression with single-nucleotide resolution requires localizing the sequences of expressed RNA transcripts within a cell in situ. Here, we describe fluorescent in situ RNA sequencing (FISSEQ), in which stably cross-linked complementary DNA (cDNA) amplicons are sequenced within a biological sample. Using 30-base reads from 8102 genes in situ, we examined RNA expression and localization in human primary fibroblasts with a simulated wound-healing assay. FISSEQ is compatible with tissue sections and whole-mount embryos and reduces the limitations of optical resolution and noisy signals on single-molecule detection. Our platform enables massively parallel detection of genetic elements, including gene transcripts and molecular barcodes, and can be used to investigate cellular phenotype, gene regulation, and environment in situ.

The spatial organization of gene expression can be observed within a single cell, tissue, and organism, but the existing RNA localization methods are limited to a handful of genes per specimen, making it costly and laborious to localize RNA transcriptome-wide (*1*–*3*). We originally proposed fluorescent in situ sequencing (FISSEQ) in 2003 and subsequently developed methods to sequence DNA amplicons on a solid substrate for genome and transcriptome sequencing (*4*–*7*); however, sequencing the cellular RNA in situ for gene expression profiling requires a spatially structured sequencing library and an imaging method capable of resolving the amplicons.

We report here the next generation of FISSEQ. To generate cDNA amplicons within the cell (fig. S1), RNA was reverse-transcribed in fixed cells with tagged random hexamers (fig. S2A). We incorporated aminoallyl deoxyuridine 5′-triphosphate (dUTP) during reverse transcription (RT) (fig. S2B) and refixed the cells using BS(PEG)9, an amine-reactive linker with a 4-nm spacer. The cDNA fragments were then circularized before rolling circle amplification (RCA) (fig. S2C), and BS(PEG)9 was used to cross-link the RCA amplicons containing aminoallyl dUTP (fig. S2, D and E). We found that random hexamer-primed RT was inefficient (fig. S3A), but cDNA circularization was complete within hours (fig. S3, B to D). The result was single-stranded DNA nanoballs 200 to 400 nm in diameter (fig. S4A), consisting of numerous tandem repeats of the cDNA sequence. BS(PEG)9 reduced nonspecific probe binding (fig. S4B), and amplicons were highly fluorescent after probe hybridization (fig. S4C). As a result, the amplicons could be rehybridized many times, with minimal changes in their signal-to-noise ratio or position (fig. S4, D and E). Using SOLiD sequencing by ligation (fig. S5), the signal overlap over 27 consecutive sequencing reactions was ~600 nm in diameter (fig. S4F). In induced pluripotent stem (iPS) cells, the amplicons counterstained subcellular structures, such as the plasma membrane, the nuclear membrane, the nucleolus, and the chromatin (Fig. 1A, fig. S6, and movies S1 to S3). We were able to generate RNA sequencing libraries in different cell types, tissue

[1]Wyss Institute, Harvard Medical School, Boston, MA 02115, USA. [2]Department of Genetics, Harvard Medical School, Boston, MA 02115, USA. [3]Department of Stem Cell and Regenerative Biology, Harvard University, Boston, MA 02138, USA. [4]Department of Systems Biology, Harvard Medical School, Boston, MA 02115, USA. [5]Allen Institute for Brain Science, Seattle, WA 98103, USA.

*These authors contributed equally to this work.
†Corresponding author. E-mail: jehyuklee@mac.com (J.H.L.); gchurch@genetics.med.harvard.edu (G.M.C.)